PERGAMON

Micron 32 (2001) 749–755

micron

www.elsevier.com/locate/micron

Atom probe tomography of 15Kh2MFA Cr–Mo–V steel surveillance specimens ☆

M.K. Miller[a,*], K.F. Russell[a], J. Kocik[b], E. Keilova[b]

[a]*Microscopy and Microanalytical Sciences Group, Metals and Ceramics Division,Oak Ridge National Laboratory, PO Box 2008, Oak Ridge, TN 37831-6136, USA*

[b]*Nuclear Research Institute Rez plc, 250 68 Rez near Prague, Czech Republic*

Abstract

An atom probe study has been performed on 15Kh2MFA base and 10KhMFT weld metal surveillance specimens from a VVER-440/213C reactor to investigate the mechanisms that produce embrittlement in low copper materials during service. The composition of the base metal was Fe-0.06 at.% Cu, 3.1% Cr, 0.34% V, 0.46% Mn, 0.35% Mo, 0.07% Ni, 0.34% Si, 0.74% C, 0.025% P, and 0.028% S. The base material was characterized after thermal aging for 10 years at 295°C and after neutron irradiation at 270°C for 10 years to a fluence of 1.0×10^{25} m^{-2} ($E > 0.5$ MeV). The ductile-to-brittle transition temperatures (DBTT) of the base metal were −49, −70 and 141°C, for the unirradiated, thermally aged and neutron irradiated conditions, respectively. The composition of the weld metal was Fe-0.05 at.% Cu, 1.46% Cr, 0.22% V, 1.11% Mn, 0.29% Mo, 1.17% Si, 0.17% C, 0.02% P, and 0.029% S. The weld material was characterized after tempering for 18 h at 690°C plus a simulated stress relief treatment of 43.5 h at 680°C, after thermal aging for 5 years at 295°C, and after neutron irradiation at 275°C for 5 years to a fluence of 5.2×10^{24} m^2 ($E > 0.5$ MeV). The DBTTs were 7, 11 and 123°C, respectively, for these three conditions. A high number density of ultrafine manganese- and silicon-enriched regions was observed in both neutron-irradiated materials. Phosphorus segregation was observed at the VC-matrix interface and at grain boundaries. Published by Elsevier Science Ltd.

Keywords: Pressure vessel steels; Neutron irradiation; Embrittlement; Precipitation; Grain boundary segregation; Atom probe tomography

1. Introduction

The pressure vessels used in nuclear reactors generally become embrittled during service due to the interaction of radiation-produced defects with the solutes in the steel. There is a general trend that the shift in the ductile-to-brittle transition temperature (DBTT) increases with the copper content of the steel. Also, this embrittlement has been linked experimentally to the formation of ultrafine (<2 nm diameter) copper-enriched precipitates in a number of copper-containing steels from both Western- and Russian-type reactors (Miller et al., 2000). These copper-enriched precipitates also contain elevated levels of nickel, manganese, silicon and phosphorus. Most of the reactor pressure vessel materials that have been characterized with the atom probe contain elevated levels of copper. This elevated copper level arises from the use of copper-coated welding wires during the fabrication of the pressure vessel (or simulations thereof). Therefore, there are a limited number of steels with low copper contents for which there is mechanical property data or microstructural information. Several other microstructural features have been observed in these materials including phosphorus clusters, ultrafine carbides, nitrides and oxides and solute segregation to grain and lath boundaries and to dislocations. A review of the contributions of the atom probe technique to the understanding of the changes that occur in pressure vessel steels during neutron irradiation has been presented recently by Miller et al. (2000).

In this study, the mechanical properties and the microstructure of low copper (~0.06 at.% Cu) base and weld materials from a Russian-type reactor have been characterized. This low copper level should minimize or eliminate the formation of the copper-enriched precipitates in the intragranular regions and thereby possibly permit the other solutes associated with these precipitates to be involved in other reactions. Materials were selected from a standard surveillance specimen program assembly of a VVER-440 power reactor.

☆ The submitted manuscript has been authored by a contractor of the US Government under Contract No. DE-AC05-96OR22464. Accordingly, the US Government retains a nonexclusive, royalty-free license to publish or reproduce the published form of this contribution, or allow others to do so, for US Government purposes.

* Corresponding author. Tel.: +1-865-574-4719; fax: +1-865-241-3650.
E-mail address: millermk@ornl.gov (M.K. Miller).

0968–4328/01/$ - see front matter Published by Elsevier Science Ltd.
PII: S0968-4328(00)00082-2

Table 1
Compositions of the base (15Kh2MFAA) and weld (10KhMFT) materials. The balance is iron

Element	Base material (15Kh2MFAA)		Weld material (10KhMFT)	
	Mass %	Atomic %	Mass %	Atomic %
Cu	0.07	0.06	0.06	0.05
Cr	2.9	3.1	1.37	1.46
Mo	0.66	0.35	0.50	0.29
Mn	0.46	0.46	1.10	1.11
V	0.31	0.34	0.20	0.22
Ni	0.07	0.07	–	–
Si	0.17	0.34	0.59	1.17
C	0.16	0.74	0.037	0.17
S	0.016	0.028	0.017	0.029
P	0.014	0.025	0.012	0.020

The primary microstructural characterization techniques that have been used in this study are atom probe field ion microscopy (APFIM) and atom probe tomography (APT). In APT, the three-dimensional coordinates and the identities of the atoms in a small volume may be determined with near atomic precision. The size, shape and composition of ultrafine features may be determined from the spatial distribution of the atoms. In addition, quantitative estimates of the solute content of the matrix may also be determined. A full description of the APT technique may be found in a monograph by Miller (2000).

2. Experimental

The compositions of the 15Kh2MFA base and 10KhMFT weld specimens used in this study are given in Table 1. The copper level in these materials is ~0.06 at.% Cu. The nickel level of 0.07 at.% in the base material was significantly lower than that present (~0.5 at.% Ni) in a typical A533B type pressure vessel steel. There was no nickel in the weld material. All compositions quoted in this paper are given in atomic percent.

The base material was initially annealed at 1000°C and quenched into oil at 125°C. The base material was characterized in the atom probe in three conditions: (1) after tempering for 18 h at 690°C plus a simulated multi-step stress relief treatment of 6 + 6 + 11 + 10.5 h at 680°C; (2) after neutron irradiation at 270°C for 10 years to a fluence of 1.0×10^{25} m^{-2} (E > 0.5 MeV, flux = 3.8×10^{16} m^{-2} s^{-1}); and (3) after thermal aging for 10 years at 295°C. In this paper, these treatments will be referred to as unirradiated, neutron irradiated and thermally aged conditions, respectively. The weld material was also examined in three conditions: (1) after welding and a simulated multi-step stress relief treatment 6 + 6 + 11 + 10.5 h at 680°C; (2) after neutron irradiation at 275°C for 5 years to a fluence of 5.2×10^{24} m^{-2} (E > 0.5 MeV, flux = 3.8×10^{16} m^{-2} s^{-1}); and (3) after thermal aging for 5 years at 295°C.

In both materials, the samples were irradiated in positions for surveillance specimens in vertical channels welded to the outer surface of the core barrel of the VVER-440 reactor. The fluences for the Charpy V-notch specimens and the tensile specimens were slightly different due to their different positions in the surveillance capsules. The neutron fluences for the base material were 9.3 and 9.0×10^{24} m^{-2} (E > 0.5 MeV) for the Charpy V-notch and tensile specimens, respectively. The neutron fluences for the weld metal were 5.2 and 4.7×10^{24} m^{-2} (E > 0.5 MeV) for the Charpy V-notch and tensile specimens, respectively.

Mechanical properties testing was performed at NRI Rez, plc as a part of the standard surveillance specimen program evaluation. To obtain a thorough understanding of the radiation embrittlement processes that occur in surveillance

Table 2
Summary of the mechanical properties of the base and weld metals for the unirradiated, thermally aged and neutron irradiated conditions

Material	State	DBTT (°C)	Yield strength (MPa)		Ultimate tensile strength (MPa)		Elongation[a] (%)		Reduction of area (%)	
			25°C	265°C	25°C	265°C	25°C	265°C	25°C	265°C
Base	Unirradiated	− 49	527	458	639	535	13.8	10.0	81	77
Base	Irradiated 10 years	141	879	760	880	779	2.2	4.2	5	27
Base	Aged 10 years	− 70	526	470	631	534	14.7	9.9	79	78
Weld	Unirradiated	7	475	377	600	491	17.9	13.2	72	71
Weld	Irradiated 5 years	123	750	646	761	708	6.4	4.9	16	16
Weld	Aged 5 years	11	483	407	593	514	15.6	12.7	70.4	67.6

[a] The elongation A_{10} is given in the table.

specimens, transmission electron microscopy (TEM) and positron annihilation spectroscopy (PAS) studies have been also performed (Kocik et al., in press).

The microstructures of the materials were characterized in the Oak Ridge National Laboratory (ORNL) energy-compensated atom probe (ECAP) and energy-compensated optical position-sensitive atom probe (ECOPoSAP). Specimens were fabricated from electropolished small bars cut from Charpy V-notch samples. All atom probe analyses were performed with a specimen temperature of 50 K, a pulse fraction of 20% and a pulse repetition rate of 1500 Hz. Field ion micrographs were recorded with neon as the image gas and with a specimen temperature of 50 K. Details of the atom probe technique and the specimen preparation methods may be found in Miller (2000).

3. Mechanical properties

A summary of the mechanical properties of the base and weld metal for all conditions is given in Table 2. The ductile-to-brittle transition temperature was measured at the level 50 J cm^{-2} (corresponding to ~41 J) with the use of an ISO pendulum. The tensile test results were determined at both room temperature (25°C) and at an elevated temperature of 265°C. A comparison of the tensile and Charpy V-notch test results indicates that the unirradiated and thermally aged materials were similar for the base material. However, significant differences in all the mechanical properties were observed between the unirradiated and neutron irradiated materials. Significant increases in the yield and ultimate tensile strengths and reductions in the elongation and reduction in area were observed after neutron irradiation. In addition, the DBTT of the base metal increased from −49 to 141°C for the unirradiated and neutron irradiated conditions, respectively. Similar trends were also observed in the weld material. The DBTT temperature of the weld metal increased from 7 to 123°C for the unirradiated and neutron irradiated conditions, respectively. These shifts in the DBTTs are similar to those measured in other pressure vessel steels irradiated to comparable fluences.

4. General microstructure

4.1. Matrix and matrix defects

The tempered bainitic-ferritic microstructures are typical for both materials under the study (Törrönen, 1979; Kocik and Keilova, 1998). The microstructure of the base metal can be classified as a mixture of tempered granular and lath bainite, with a small amount of ferrite. The weld metal microstructure consists predominantly of acicular ferrite in addition to small amount of bainite and a network of proeutectoid ferrite.

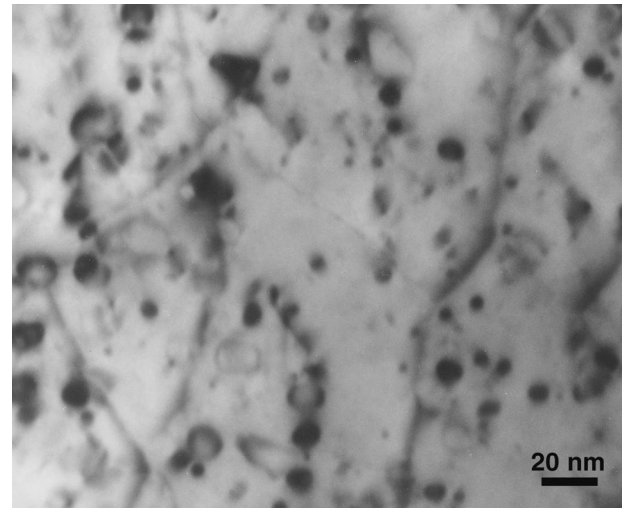

Fig. 1. Transmission electron micrograph of dislocations, dislocation loops and vanadium carbides in the neutron irradiated base material.

The defect population induced by neutron irradiation in the surveillance specimens and visible in the transmission electron microscope consists of 'black dots', small dislocation loops and fine precipitates, concentrated to dislocations and low-angle boundaries, as shown in Fig. 1. It is believed that the 'black dots' involve vacancy-solute complexes, in addition to unresolved small loops and precipitates. The size of the dislocation loops increased, and the number density of the 'black dots' decreased, with increasing neutron fluence. In addition, only very weak recovery of dislocation substructure occurs. Aging for 10 years at the reactor service temperature results in an advanced polygonization of the dislocation substructure.

4.2. Carbides

Transmission electron microscopy revealed that blocky chromium-rich carbides of the M_7C_3 and $M_{23}C_6$, type, typically ≈ 200 nm in size, precipitate preferentially along boundaries. An atom probe analysis of a M_7C_3 carbide in the thermally aged base material yielded a composition of 41.7 ± 2.0% Cr, 23.1 ± 1.5% Fe, 3.4 ± 0.6% V, 1.7 ± 0.4% Mn, 0.3 ± 0.17% Mo, 0.3 ± 0.17% Si + N, and 29.5 ± 1.7% C. No phosphorus was found in this carbide. This result is in agreement with a previous atom probe analysis of a M_7C_3 carbide in a weld in a VVER 400 reactor (Miller et al., 1995a).

In addition, transmission electron microscopy revealed that fine plate-like VC carbides, less than 20 nm in size, precipitated homogeneously within the microstructure, in both base and weld metals. A small shift in VC precipitate size distribution towards the larger particles was observed in materials aged for 10 years (Kocik et al., 2000, in press).

Field ion micrographs of vanadium carbide precipitates are shown in Fig. 2. These carbides exhibit bright contrast

Table 3
Compositions of vanadium carbide precipitates as determined by atom probe field ion microscopy. The results are in atomic percent

	V	Cr	Mo	Fe	C	N
Thermally aged base material	40.6 ± 1.8	9.3 ± 0.9	4.9 ± 0.6	0.24 ± 0.14	42.9 ± 1.9	2.1 ± 0.4
Unirradiated weld	40.2 ± 2.6	8.9 ± 1.2	9.2 ± 1.2	1.1 ± 0.4	36.8 ± 2.5	3.6 ± 0.8
Thermally aged weld	42.0 ± 2.7	6.5 ± 1.1	4.2 ± 0.9	2.3 ± 0.6	36.7 ± 2.5	8.4 ± 1.2

compared to the surrounding matrix. The full extent of the precipitate is shown in Fig. 2(a) and (c). The size of these precipitates was found to range from ~5 to ~10 nm. Although a systematic study of these carbides was not performed, the compositions of some of the precipitates analyzed are given in Table 3. An atom map of a volume containing a vanadium carbide precipitate in the thermally aged weld is shown in Fig. 3. Phosphorus segregation is evident at the precipitate–matrix interface.

4.3. Boundaries

Since the grain size of these materials was large compared to the volume of analysis in an APT specimen and no preselection of atom probe specimens was performed in the transmission electron microscope, only limited data were obtained from grain boundaries. A field ion micrograph of a boundary in the thermally aged weld material is shown in Fig. 4. The brightly-imaging atoms indicate significant solute segregation at the grain boundary. Significant enrichments of phosphorus and carbon were measured. The Gibbsian interfacial excesses were determined to be $\Gamma_P = 2.4 \times 10^{14}$ atoms cm^{-2} (coverage ~30% of a monolayer) and $\Gamma_C = 5.0 \times 10^{14}$ atoms cm^{-2} (coverage ~14% of a monolayer). These results are similar to previous atom probe characterizations of boundaries in other welds from Russian VVER 400 reactors (Miller et al., 1995a,b; Miller and Russell, 1996).

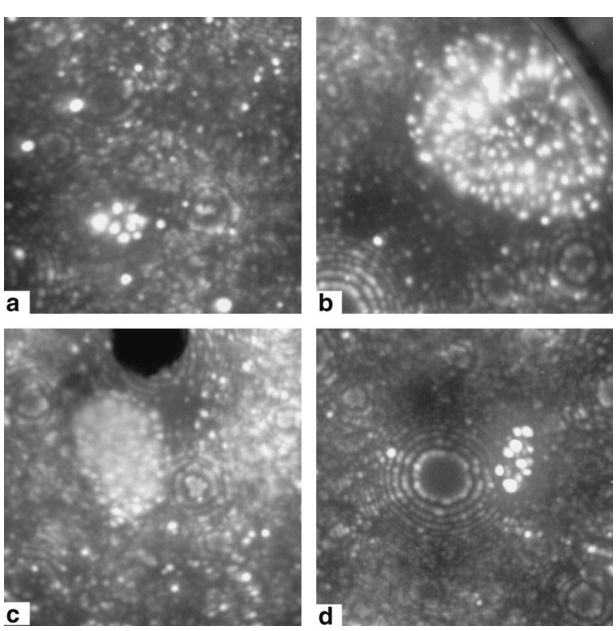

Fig. 2. Field ion micrographs of vanadium carbide precipitates in: (a) unirradiated weld; (b) thermally aged weld; (c) thermally aged base material and; (d) neutron irradiated base material.

5. Intragranular microstructure

The matrix compositions of the base material and weld materials were determined for each condition. In these atom probe estimates, the volumes of analysis were obtained from ferritic or bainitic regions, which contained no other features such as second phases, boundaries or dislocations. The results are summarized in Table 4. The results indicate that the copper level in the matrix under all conditions examined is similar to the bulk copper content of the alloys. Reductions in the chromium, vanadium and carbon levels with respect to the bulk contents were observed in the matrices, which are consistent with these elements partitioning to chromium-enriched M_7C_3, $M_{23}C_6$, and VC carbides during the processing of the steels prior to irradiation.

The most significant difference between the unirradiated/thermally aged and neutron-irradiated materials was the presence of a high number density of manganese- and

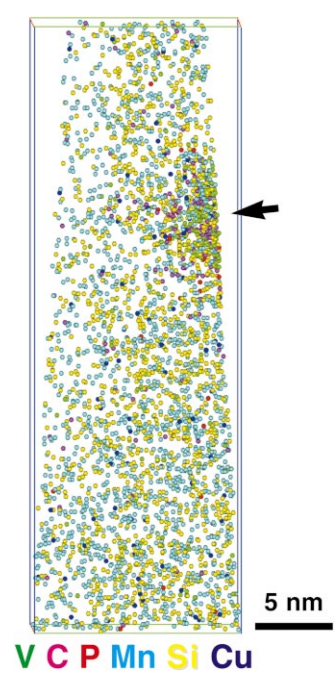

Fig. 3. Three-dimensional atom probe atom map of a volume of the thermally aged weld material containing a vanadium carbide precipitate. Phosphorus segregation is evident at the precipitate–matrix interface.

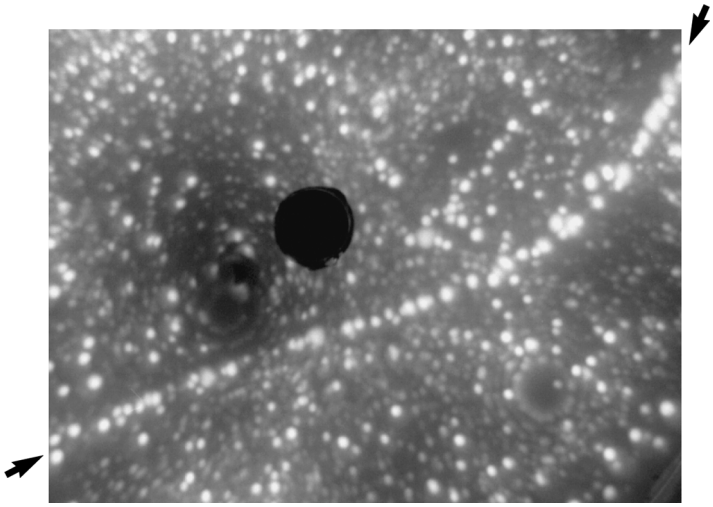

Fig. 4. Field ion micrograph of a decorated grain boundary in thermally aged weld. Enrichments of carbon and phosphorus were measured at the boundary.

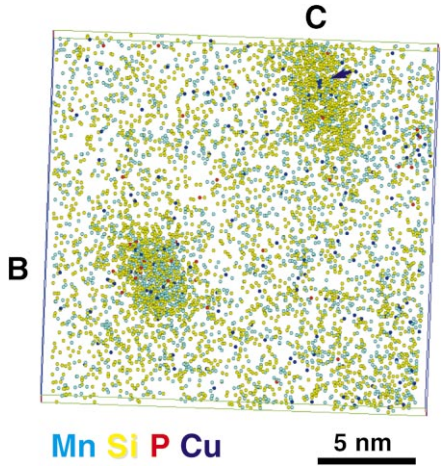

Fig. 5. Three-dimensional atom probe atom map of a volume of the neutron irradiated weld material containing two spherical manganese- and silicon-enriched features designated B and C. The copper core of feature C is indicated by the arrow.

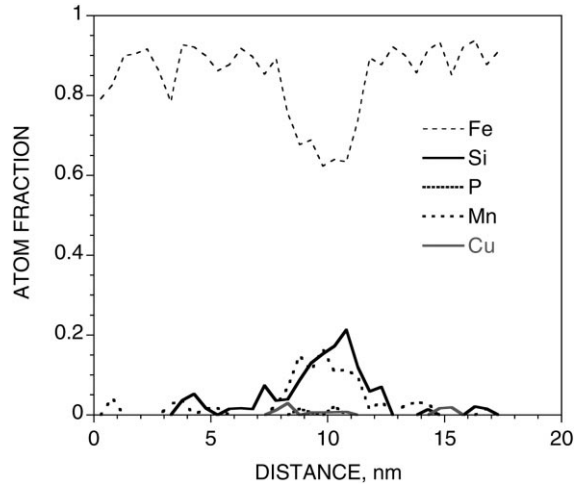

Fig. 6. Composition profile through the core of feature B. Note the enrichments of manganese, silicon, copper and phosphorus and the depletion of iron in the feature.

Table 4
Average compositions of the matrix as determined by atom probe field ion microscopy and atom probe tomography. The balance is iron and the results are in atomic percent with a 2σ error

	Base material (15Kh2MFAA)			Weld material (10KhMFT)		
	Unirradiated	Thermally aged	Neutron irradiated	Unirradiated	Thermally aged	Neutron irradiated
Cu	0.06 ± 0.02	0.05 ± 0.02	0.06 ± 0.009	0.05 ± 0.01	0.05 ± 0.006	0.05 ± 0.009
Cr	1.82 ± 0.12	2.47 ± 0.20	2.19 ± 0.05	1.29 ± 0.05	1.13 ± 0.03	1.33 ± 0.04
Mo	0.29 ± 0.05	0.39 ± 0.08	0.31 ± 0.02	0.30 ± 0.02	0.23 ± 0.01	0.37 ± 0.02
Mn	0.32 ± 0.05	0.51 ± 0.09	0.31 ± 0.02	0.88 ± 0.04	1.00 ± 0.02	1.08 ± 0.04
V	0.10 ± 0.02	0.23 ± 0.06	0.15 ± 0.01	0.08 ± 0.01	0.04 ± 0.006	0.08 ± 0.01
Si	0.52 ± 0.06	0.34 ± 0.07	0.16 ± 0.01	1.21 ± 0.05	1.19 ± 0.03	1.22 ± 0.04
C	0.017 ± 0.017	0	0.17 ± 0.001	0.05 ± 0.01	0.05 ± 0.06	0.17 ± 0.02
P	0.017 ± 0.017	0.033 ± 0.033	0.037 ± 0.006	0.04 ± 0.01	0.012 ± 0.003	0.039 ± 0.003

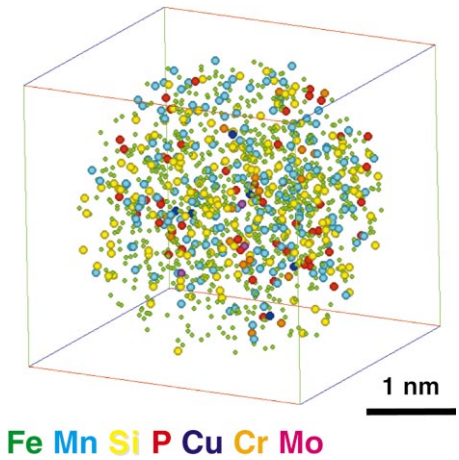

Fig. 7. Three-dimensional atom probe atom map of the core of a spherical manganese- and silicon-enriched feature in the neutron irradiated weld. All atoms are shown.

silicon-enriched features in the matrix. Examples of atom maps of two roughly spherical features (B and C) in the neutron-irradiated weld material are shown in Fig. 5. A composition profile through feature B is shown in Fig. 6. An atom map of all the atoms in the core region (1.5 nm in diameter) of feature B is shown in Fig. 7. Although the iron level in the core region of these features is depleted with respect to the surrounding matrix, it is still is high. A pair of cylindrical regions (D and E) is shown in Fig. 8. Examples of atom maps of two spherical (F and H) and a cylindrical feature (G) in the neutron-irradiated base material are shown in Figs. 9 and 10. The cylindrical feature (G) intersects a vanadium carbide precipitate. The size of the spherical features was approximately 3–4 nm in diameter. The cylindrical features exhibited similar diameters and always extended further than the volume of analysis. The compositions of volume elements taken from the cores of these features are given in Table 5. It is

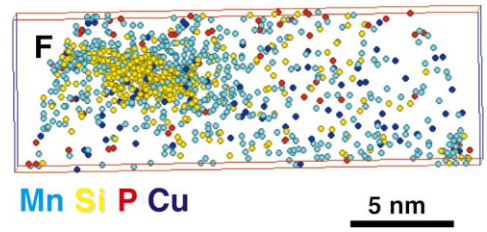

Fig. 9. Atom map of a spherical manganese- and silicon-enriched feature designated F in neutron irradiated base material.

evident from these compositions and the atom maps that there were also significant enrichments of copper, phosphorus and carbon in these features. Due to the relatively small enrichments of these elements, the matrix composition is only changed by a small amount. The manganese and silicon levels in these features were found to extend over a significant range of concentrations but no distinct correlation with morphology was observed.

These features exhibited two distinct morphologies, roughly spherical and cylindrical. A simple explanation for the extended cylindrical morphology is solute segregation to dislocations resulting in the formation of atmospheres similar to Cottrell atmospheres in the stress field associated with the dislocation. It is also possible that some of the spherical features could arise from solute segregation to small dislocation loops or other small defects such as vacancy clusters or nanovoids. An alternative possibility is that some of the spherical features initially form through the clustering of copper atoms and these embryos then attract the other solutes. Evidence of a copper core consisting of a few (~5) copper atoms has been observed in some of the features, for example, feature C in Fig. 5. These solute enriched regions will significantly impede the motion of dislocations and thereby account for the changes observed in the mechanical properties.

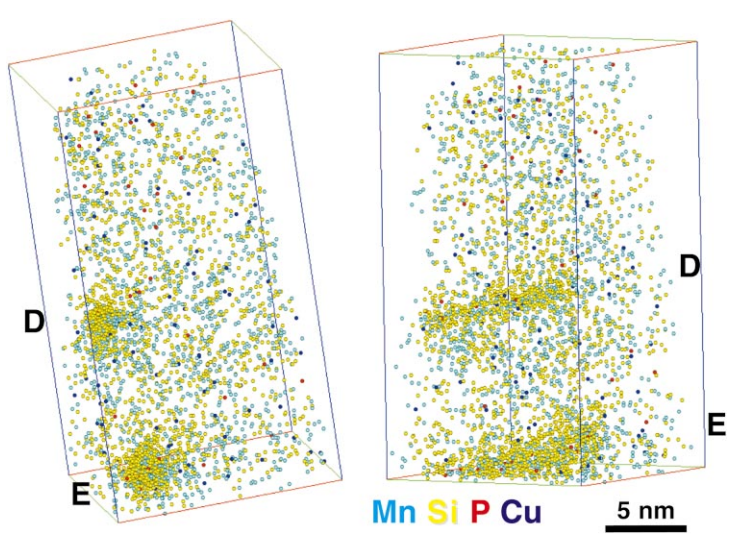

Fig. 8. Three-dimensional atom probe atom map of a volume of the neutron irradiated weld containing two cylindrical manganese- and silicon-enriched features designated D and E. The volume has been rotated to show both side and end views of the features.

Table 5
Compositions of the Mn- and Si-enriched features in neutron-irradiated base and weld materials. The balance is iron and the results are in atomic percent

	Cu	Cr	Mo	Mn	V	Si	C	P	Shape
Base									
F	0.79	2.36	0.09	3.40	–	15.4	–	–	Sphere
G	0.46	3.68	0.13	2.50	0.07	4.14	0.13	0.13	Sphere
H	0.23	2.57	0.38	2.80	0.15	3.03	0.38	0.30	Cylinder
Weld									
A	0.46	1.55	0.31	14.5	0.08	14.4	–	3.79	Sphere
B	0.56	0.79	0.56	12.1	–	12.7	–	0.56	Sphere
C	0.82	0.37	0.09	2.20	–	16.7	–	0.09	Sphere
D	0.29	1.29	0.05	3.68	0.05	11.5	0.14	0.19	Cylinder
E	0.04	1.43	0.35	4.62	–	12.0	0.09	0.48	Cylinder

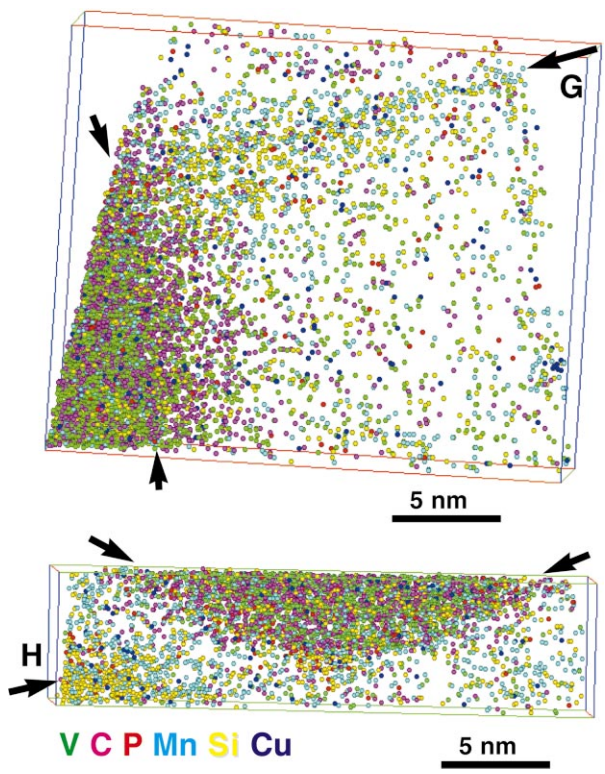

Fig. 10. Atom maps of cylindrical (G) and spherical (H) manganese- and silicon-enriched features near vanadium carbide precipitates in the neutron irradiated base material.

6. Conclusions

This investigation has determined that there were significant increases in the yield and ultimate tensile strengths and reductions in the elongation and reduction in area in both base and weld materials after neutron irradiation. In addition, the ductile-to-brittle transition temperatures increased significantly after neutron irradiation. These changes in mechanical properties correlate with the presence of spherical and cylindrical manganese-, silicon-, copper-, phosphorus- and carbon-enriched features in the matrix of the neutron irradiated base and weld materials.

Acknowledgements

Research at the Oak Ridge National Laboratory SHaRE User Facility was sponsored by the Division of Materials Sciences and Engineering, US Department of Energy, under contract DE-AC05-96OR22464 with Lockheed Martin Energy Research Corp. and by the Office of Nuclear Regulatory Research, US Nuclear Regulatory Commission under inter-agency agreement DOE 1886-N695-3W with the US Department of Energy. The transmission electron microscopy research at the Nuclear Research Institute Rez plc. was sponsored by the Czech Academy of Sciences under Grant No. 106/96/1319.

References

Kocik, J., Keilova, E., 1998. Microstructure of Cr–Mo–V reactor pressure vessel steels. NRI Research Bulletin, Nucleon, No. 3, Rez, p. 19.

Kocik, J., Keilova, E., Prochazka, I., Cizek, J., 2000. In: Hamilton, M.L., Kumar, A.S., Rosinski, S.T., Grossbeck, M.L. (Eds.), Proceedings of the 19th Symposium on Effects of Radiation on Materials, Seattle, June 1998; ASTM STP/1366, ASTM, West Conshohocken, PA, p. 354.

Kocik, J., Keilova, E., Prochazka, I., Cizek, J., 2001. J. Nucl. Mater. in press.

Miller, M.K., 2000. Atom probe tomography: analysis at the atomic level. Kluwer Academic/Plenum Press, New York.

Miller, M.K., Jayaram, R., Russell, K.F., 1995a. Characterization of phosphorus segregation in neutron-irradiated Russian pressure vessel steel weld. J. Nucl. Mater. 225, 215–224.

Miller, M.K., Jayaram, R., Russell, K.F., 1995b. Characterization of phosphorus segregation in neutron-irradiated pressure vessel steels by atom probe field ion microscopy. In: Robertson, I.M., Rehn, L.E., Zinkle, S.J., Phythian, W.J. (Eds.). Proceedings of 'Microstructure of Irradiated Materials', 29 November–1 December 1994, Boston, MA, Vol. 373. Materials Research Society, Pittsburgh, PA, pp. 113–118.

Miller, M.K., Russell, K.F., 1996. APFIM characterization of a high phosphorus Russian RPV weld. Appl. Surf. Sci. 94/95, 278–383.

Miller, M.K., Pareige, P., Burke, M.G., 2000. Understanding pressure vessel steels: an atom probe perspective. Mater. Charact. 44, 235–254.

Törrönen, K., 1979. Microstructural parameter and yield in a quench and tempered Cr–Mo–V pressure vessel steel. Materials and Processing Technology, vol. 22. Valtion Teknillinen Titkmuskeskus, Espoo, Finland, p. 1.